# Self-organization of post-implantation-like embryonic tissues from blastoids

**Authors:**
Erik J. Vrij[1,2], Yvonne Scholte op Reimer[1], Javier Frias Aldeguer[1,3], Isabel Misteli Guerreiro[3], Jop Kind[3], Bon-Kyoung Koo[2], Clemens A. Van Blitterswijk[1], Nicolas C. Rivron[1, 3]

1. Merln Institute for technology-driven regenerative medicine, Maastricht University, The Netherlands
2. IMBA - Institute of Molecular Biotechnology GmbH, Vienna, Austria
3. Hubrecht Institute for developmental biology and stem cell research, Utrecht, The Netherlands.

**Correspondence should be addressed to:**
Nicolas Rivron nicolasrivron@gmail.com
Erik Vrij erikvrij@gmail.com

## Abstract

**The early mammalian embryo (blastocyst) contains three co-developing types of stem cells. Two supporting extraembryonic types - the trophectoderm and the primitive endoderm - encase and guide the pluripotent epiblast that eventually forms all body tissues. Unlike embryos, stem cell-based models of the embryo can be generated in large numbers and subjected to high-content screens as a basis for basic and biomedical discoveries** (Rivron et al., 2018a; Vrij et al., 2016b)**. Here, we show that aggregates of naive Embryonic stem cells cultured in chemically-defined conditions and exposed to combinatorial screens of signaling molecules, rapidly (48 hours) and efficiently (80%) set apart PrE-like cells. These cells produce a basal lamina, generate progenitors resembling both visceral and parietal endoderm, and polarize co-developing Epiblast cells to form a pro-amniotic cavity. In blastoids, stem cell-based models of the early blastocyst** (Rivron et al., 2018b)**, this combination of signals increases the ratio and number of Gata6+/Nanog+ cells and promotes the survival, growth and morphogenesis of a post-implantation-like Epiblast *in vitro*. Modeling early embryonic development in chemically-defined *in vitro* conditions shows that the primitive endoderm forms *via* a specific combination of signaling pathways and sufficient to drive the development of the Epiblast.**

## Introduction

The mouse embryo consists of three distinct lineages: the pluripotent Epi (Epi) that develop into the fetus, and two extraembryonic lineages—trophoblast and primitive endoderm (PrE) — sustaining the development of the embryo. At the E3.5 stage, the inner cell mass of the blastocyst bifurcates to establish the PrE and Epi compartments (Chazaud et al., 2006; Onishi and Zandstra, 2015; Schrode et al., 2014). This occurs in a seemingly self-organizing manner driven by a intercellular signaling circuitries (e.g. FGF/Mapk/Erk signalling pathway), which adjusts the cell numbers mutually allocated to the pluripotent Epi or PrE (Onishi and Zandstra, 2015; Yamanaka et al., 2010).

The formation of PrE and its derivatives is studied using Embryoid bodies (EBs); aggregates of embryonic stem cells (ESCs) that mimic aspects of early embryonic development (Brickman and Serup, 2017; Doetschman et al., 1985;

Hamazaki et al., 2004). However, EBs are formed in chemically-undefined conditions and PrE is not generated efficiently, which occlude studying underlying mechanisms.

Recently, we reported the generation of blastoids (Rivron et al., 2018b), embryonic stem cell (ESC) and trophoblast stem cell (TSC)-based structures resembling the E3.5 blastocyst. Building on previous observations (Gardner, 2000), this model proposed a range of inductive signals originating from the embryo and regulating trophectoderm development and implantation. Here, we investigate the role of signaling pathways forming the PrE under chemically-defined conditions, and its influence on post-implantation development of blastoids.

## Results

**Naïve pluripotency increase PrE differentiation.**

We used a high-content screening platform of non-adherent hydrogel microwells in 96 well-plates (Vrij et al., 2016a) to reproducibly aggregate small number of ESCs into EBs (**Figure 1A**). ESCs seeded into microwells were normally distributed across the 430 microwells within each well (7–12 cells per microwell) and formed EBs within 24 hours (**Figure 1B, S1)**. We quantified PrE differentiation *via* in situ imaging of fluorescent reporters Pdgfrα (ESCs $^{Pdgfr\alpha\text{-}h2b\text{-}gfp/+}$) (Artus et al., 2010; Plusa et al., 2008) or Gata6 ESCs $^{Gata6\text{-}h2b\text{-}venus/+}$). Leukemia inhibitory factor (Lif) appeared essential for the viability of EBs when formed with low cell numbers in serum-free B27N2 medium. However, EBs did not proliferate and formed only few PrE cells (1% and 4% of Pdgfrα+ EBs for 2D expansion in B27N2/2i/Lif and serum/Lif, respectively (**Figure 1C**). In contrast, serum/Lif induced proliferation and expression of Pdgfrα+ EBs (44%, **Figure 1C**, $p < 0.001$, ANOVA with Tukey's multiple comparison test). Consistent with previous reports (Schröter et al., 2015), we observed that an initial 2D expansion in 2i/Lif B27N2 medium was more permissive for PrE formation as compared to serum-containing medium (**Figure 1C**). We concluded that similar to the blastocyst (Artus et al., 2010; Plusa et al., 2008), PrE formation from ESCs requires a permissive naïve state along with unknown signals regulating proliferation and differentiation.

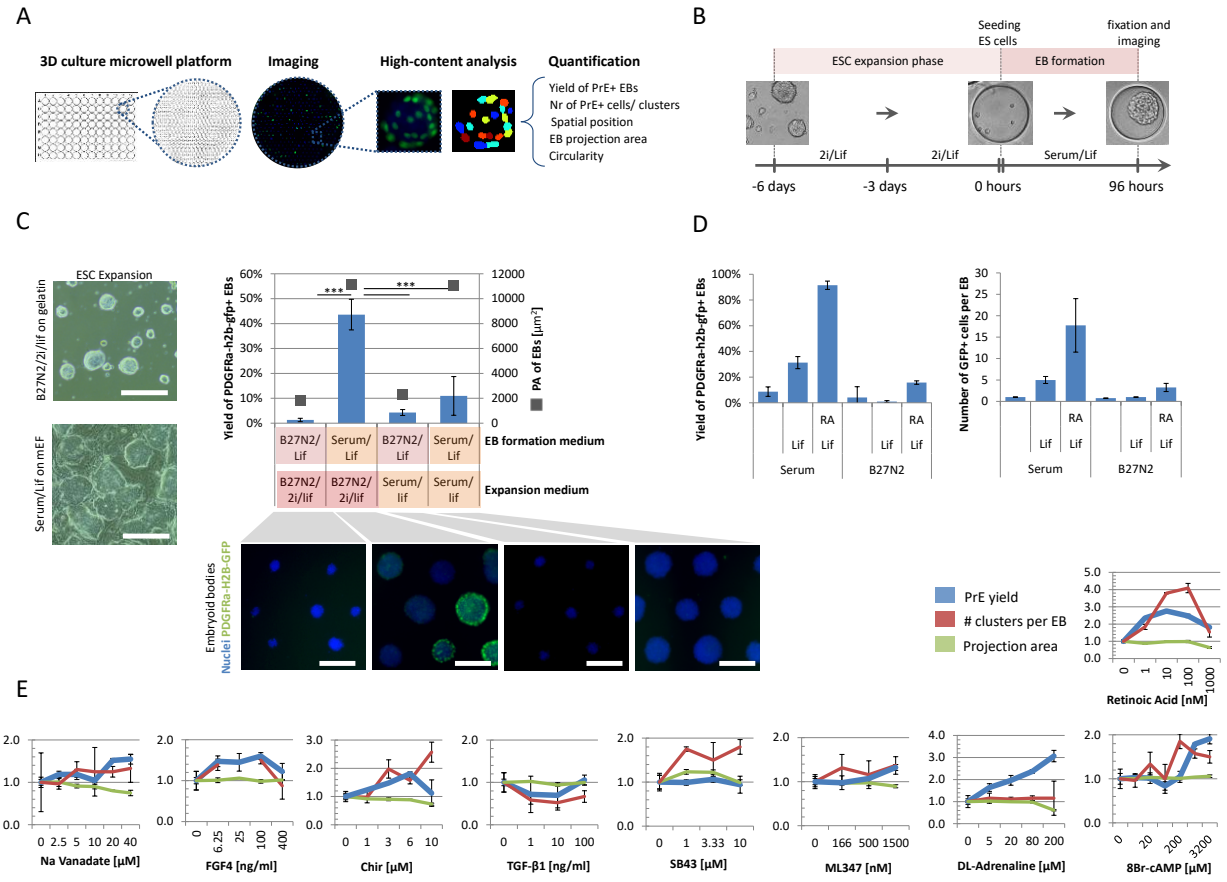


**Figure 1:** Naïve pluripotency permits efficient extraembryonic differentiation in embryoid bodies (EBs). (A) High-content screening (HCS) methodology of 96-well plates that are imprinted with agarose microwell arrays (430 microwells per well) in which EBs are formed, cultured and imaged (each microwell capturing a single EB). (B) Schematic of experimental set-up including ESC expansion and EB-based primitive endoderm (PrE) differentiation. (C) Bright-field images of ESCs expanded in serum/lif and B27N2 2i/li (left ordinate). Quantified yield of PrE-differentiation capacity in EBs derived from ESCs expanded in naïve (B27N2/2i/Lif) versus serum/Lif conditions (right ordinate). Fluorescence images (bottom) show the nuclei (blue) and Pdgfrα-h2b-gfp+ cells (green) within EBs formed in B27N2/Lif while expanded in B27N2/2i/Lif (left), EBs formed in serum/Lif while expanded in B27N2/2i/Lif (middle), and EBs formed in serum/Lif while expanded in serum/Lif on mouse embryonic fibroblast (mEF) cells (right). Scale bars represent 200 µm. (D) Yield of Pdgfra-h2b-gfp+ EBs and number of GFP+ cells per EB in B27N2 and serum medium supplemented +/- Lif and +/- RA. E) Dose response curves showing effect of soluble pathway modulators on yield of Pdgfrα-h2b-gfp+ EBs (blue), number of PrE cells per EB (red) in median focus plane (10x objective) and EB-projection area as a proxy for EB-size (green). All values were normalized to H20/DMSO controls. Average and standard deviation values were obtained from n = 3 or 4 wells with every well containing approximately 400 EBs. Imaged after 96 h of culture. In panels C and D, bars and error bars show means and standard deviations, respectively, obtained from N = 4 wells, with each well containing ~400 EBs. *** $p < 0.001$, ANOVA with Tukey's multiple comparison test.

**Signalling pathways inducing PrE-differentiation.**

Several signalling pathways influence the formation of the PrE lineage including Stat (Morgani and Brickman, 2015), Retinoic acid (Cho et al., 2012), Fgf (Chazaud et al., 2006; Yamanaka et al., 2010), Wnt (Krawetz and Kelly, 2008; Price et al., 2013), and Tgf (Niakan et al., 2013). However, how these pathways act and interact is poorly known. Lif increased the formation of Pdgfrα+ EBs (10 ng/ml Lif in serum cultures, 30% yield, 3.6-fold increase, **Figure 1D**) and Retinoic acid (RA) further improved the process (10 nM in serum culture, 91% yield, 3-fold increase,

**Figure 1D**) along with increasing the number of Pdgfrα+ cells per EB (5.5-fold, **Figure 1D)**. In contrast, the effect was restricted in serum-free B27N2/Lif medium (16% yield). We concluded that Lif and RA support but are not sufficient to form Pdgfrα+ cells.

We then created a small library of pathway activators and inhibitors (**Table 1**), tested them individually in serum-containing medium, and measured the percentage of Pdgfrα+ EBs (yield) and the number of Pdgfrα+ clusters per EB (number of clones). The broad tyrosine phosphatase inhibitor sodium orthovanadate supported a 1.5-fold increase in yield and a 1.3-fold increase in the number of clones (40 µM, **Figure 1E**). FGF4 and the Wnt activator CHIR99021 increased both the yield and the number of clones (FGF4 100 ng/mL, 44%, 1.6-folds; CHIR99021 6µM, 81%, 1.6-folds, **Figure 1E**). Inhibiting Wnt secretion (IWP2), Wnt processing (XAV), and MAPK (PD032) did not increase the yields (**Figure S3**). We concluded that, similar to events occurring in the blastocyst (Chazaud et al., 2006), the Fgf and Wnt pathways regulate the formation and the expansion of Pdgfrα+ cells.
On the contrary, the activation of the Tgfβ pathway by Nodal, Activin A, BMP4 or Tgf-β1 reduced either the yield or the number of clones. Consistent with these observations, the TGF-β receptor inhibitor SB43 and the Alk1/2 inhibitor ML347 had the opposite effect (**Figure 1E and S3)**. The BMP pathway inhibitor LDN193189 prevented proliferation of ESCs (**Figure S3**).
We concluded that the activation of the Wnt and Fgf pathways and the inhibition of the Tgfβ pathway acted on the formation of Pdgfrα+ cells.

**GPCR ligands screen**

To complement the action of the developmental pathways, we then investigated the potency of GPCR ligands and ran a compound screen of 264 small molecules. DL-adrenaline, a β-adrenergic agonist acting upstream of the cAMP/PKA pathway, increased the yield of Pdgfrα+ EBs by 206% without affecting the overall size of the EB or the number of Pdgfrα+ cells per EB (**Figure 1E**). Consistent with previously established roles of GPCR ligands (Calebiro and Jobin, 2018), we concluded that DL-adrenaline potentiate ESCs for Pdgfrα expression independent of proliferation. We confirmed that the cell-permeable analogue 8Br-cAMP also increased the yield of PrE EBs (91% at 3200 µM, **Figure 1E**)(Vrij et al., 2016b) without affecting the size of EBs.

Altogether, we concluded that Fgf4, Wnt, Lif, RA, cAMP individually increase the potential for ESCs to express Pdgfrα.

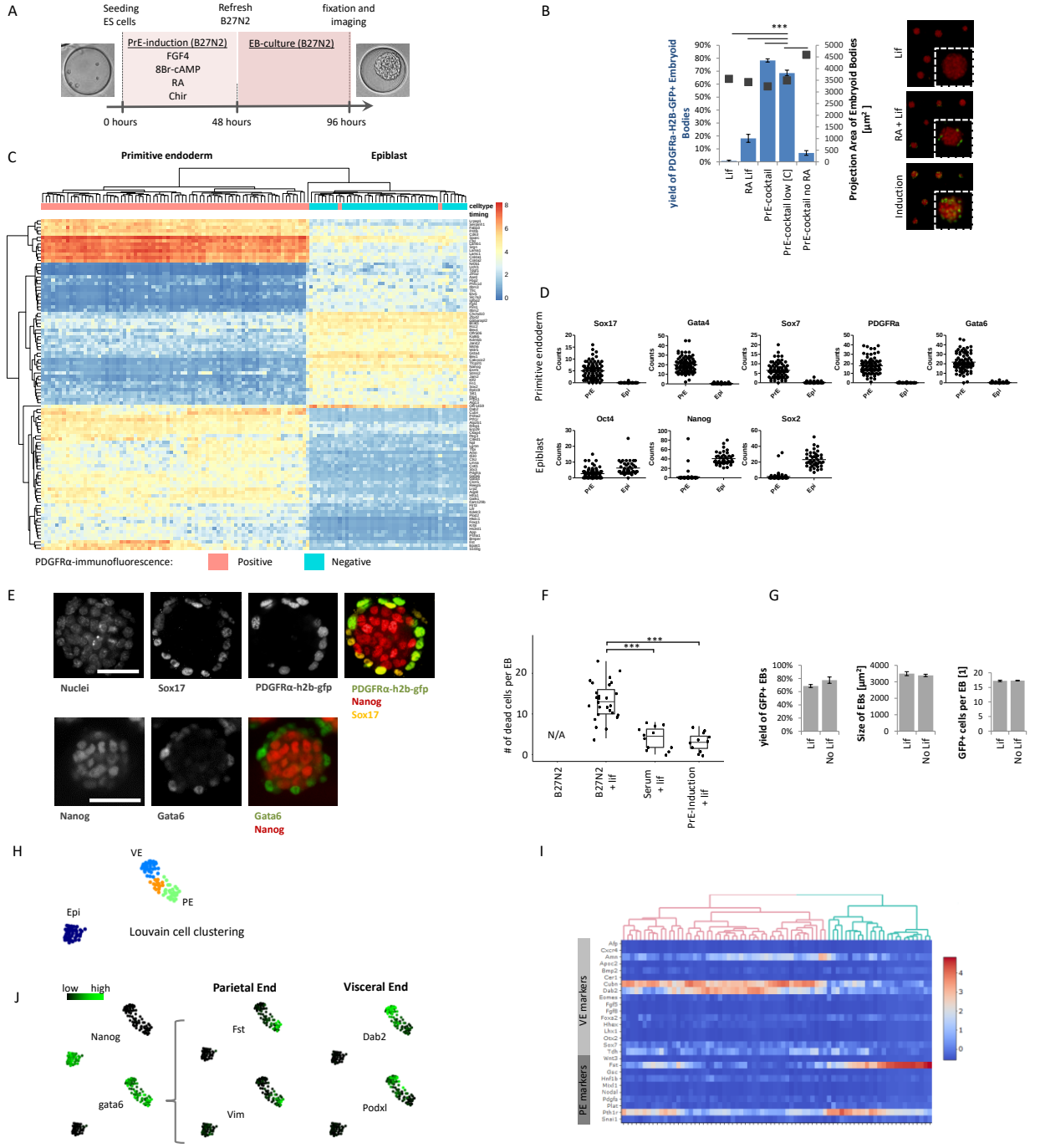


**Figure 2:** Serum-free differentiation into primitive endoderm. A) Schematic for chemically induced differentiation of EBs towards PrE. B) Yields for PrE-differentiation in EBs using the induction cocktail. Low [c] implies a lowering of concentrations from 3 M to 1 M cAMP and 6 µM to 3 µM Chir. C) Single-cell RNA sequencing data for top 100 differentially expressed genes between cells that stained positive and negative for Pdgfrα. D) Transcription factor RNA transcript levels for Pdgfrα-labelled cells (PrE) and non-labelled cells (Epi). E) immunofluorescence images of PrE-induced EBs for Gata6, Sox17, Nuclei and Pdgfrα-h2b-gfp reporter after 96 hours of culture. Scale bar represents 100 µm. F) Cell viability assay; number of dead cells (Ethidium homodimer-positive cells) per EB comparer for standard EB culture Serum + Lif and serum-free B27N2 minus Lif, with Lif and with PrE-induction cocktail including Lif. G) Yield of Pdgfrα-h2b-gfp+ EBs, size of EBs and number of Pdgfrα-h2b-gfp+ cells per EB for PrE-induction with/without Lif. H) SPRING Louvain clustering (Weinreb et al., 2016) delineates four putative

subpopulations; dark blue: E4.5 Epi, light blue: early VE, orange: subpopulation of intermediate VE/PE marker profile, early PE. I) Hierarchical clustering of Pdgfrα+ immuno-labelled cells based on VE and PE gene list (Edgar et al., 2013). J) SPRING expression patterns of PE genes Follistatin (Fst) and Vimentin (Vim), and VE genes Dab2 and Podocalyxin (Podxl/ Pcx).

**A combinatorial screen reveals a chemically-defined medium inducing Pdgfrα expression.**

Because signaling molecules act in concert to ensure development, we ran combinatorials of our molecules in serum-free medium (B27N2 medium, **Figure 2B**). Using a factorial design screening approach (Hutchens et al., 2007), we tested combinations of 8br-cAMP, DL-Adrenaline, Lif, FGF4, Sodium Vanadate, Chir, ML347, SB43 and RA, and Activin A at effective concentration ranges. Specific combinations of factors preserved EB viability (measured by EB-size), EB integrity (measured by EB circularity) and permitted PrE-like differentiation (Pdgfrα expression, **Figure S4 B**). Among all 21 combinations, a medium containing 8br-cAMP (1 M), RA (10 nM), FGF4 (100 ng/mL) and Chir (5 µM) led to a stark upregulation of the yield of PrE+ EBs (78%, **Figure 2B**). Consistent with the important role of RA, depleting this molecule from the induction medium reduced the yield significantly (**Figure 2B)**. However, the synergy with other factors was essential for a robust and efficient induction (**Figure 2B**). This chemically-defined inductive medium reduced the number of dead cells per EB as well, to levels similar to serum-containing medium (**Figure 2F**) and did not require the presence of Lif neither for maintaining viability or Pdgfrα expression (**Figure 2G**).

**The embryoid bodies concomitantly form PrE/Epi-like cells.**

The resulting EBs formed an outer layer of PrE-like cells positive for the transcription factors Gata6 and Sox17 and a core of Nanog+ cells (**Figure 2E**), which is consistent with the formation of the PrE and Epi of the blastocyst (Chazaud et al., 2006). We further characterized the cells *via* single cell transcriptomic. In congruence with Pdgfrα labelling, the cells showed two distinctive subpopulations (**Figure 2C)**. One population expressed the PrE genes Gata6, Gata4, Pdgfrα, Sox7 and Sox17, while the other one expressed the Epi genes Nanog, Sox2 and Oct4 (**Figure 2D**). SPRING Louvain clustering (Weinreb et al., 2016) indicated 3 subpopulations of PrE cells (**Figure 2H**); one displaying the parietal endoderm (PE) markers Follistatin and Vimentin, one opposing subpopulation displaying the early visceral endoderm (VE) markers Dab2 and Podocalyxin, while the third subpopulation had an intermediate profile. Principal component analysis similarly identified a compact Epi cluster and wider PrE cluster dispersed along PC2 (**Figure S5**) with PE genes such as Vim, Fst, Thbd, Sema6 and Nog on one side and VE genes such as Amn, Cubn, Dab2, Podxl (Pcx), Apoe on the opposite side of PC2. In line with this, hierarchical clustering using known markers for PrE, early VE and PE (Edgar et al., 2013) identified two subpopulations (**Figure 2I)**. Some more differentiated VE markers such as Apoa1 and Afp, and PE markers such as Krt1 (Cytokeratin Endo C) were not found, which suggests a PrE cell population transiting into bifurcating VE and PE states.

In accordance with the polarized epithelium of the VE and its tgf-β modulating function in patterning the embryo (Mesnard et al., 2006), our GO term analysis (**Figure S7, Table 2**) showed that, in the putative VE subpopulation, cell polarity regulators and Tgf-β pathway responses were enriched in this subpopulation.

All together, we concluded that the chemically-defined medium induced the co-formation of spatially organized PrE-like cells and of Epi-like cells capable of bifurcating into both VE and PE lineages.

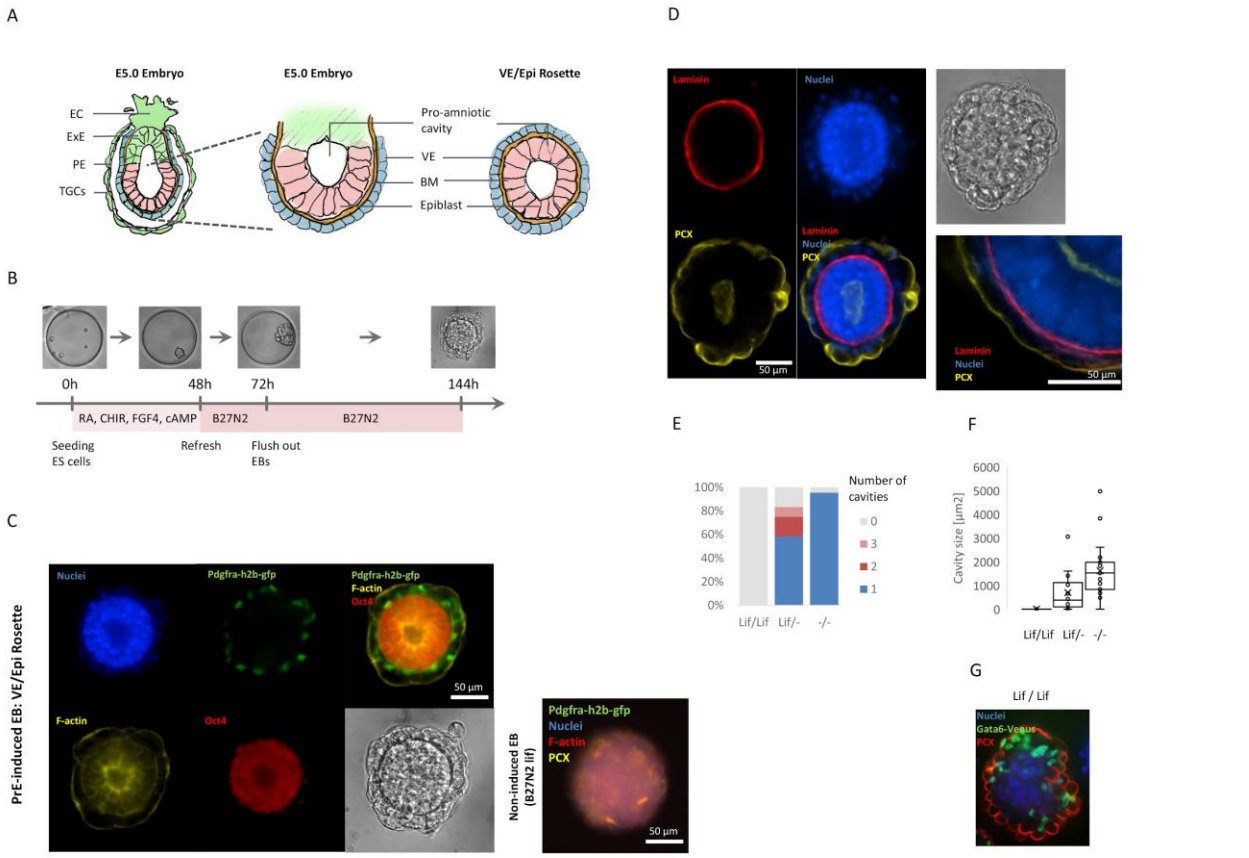


**Figure 3**: Post-implantation Epi development including extraembryonic endoderm. **A)** Schematic depicting E5.0 embryo and corresponding tissue in VE/Epi Rosette. EC = Ectoplacental Cone, ExE = Extraembryonic Ectoderm, PE = Parietal Endoderm, TGCs = Trophoblast Giant cells, VE = Visceral Endoderm, BM = Basement Membrane. **B)** Schematic on culture protocol for VE/Epi rosette formation. **C)** Immunofluorescence images for PrE-induced VE/Epi rosettes and non-induced aggregate depicting nuclei, F-actin (pro-amniotic cavity), Pdgfrα-h2b-gfp (VE) and Oct4 (pluripotent Epi). Pcx labelling shows absence of polarized cells in non-induced aggregate. **D)** Immunofluorescence images depicting cell nuclei, Pcx (polarization), Laminin (basement membrane). In grey: bright-field image of VE/Epi rosette. **E)** Effect of Lif on yield of structures forming a pro-amniotic cavity or multiple cavities. Lif/Lif indicates Lif supplementation during first 3 days of PrE-induction and subsequent 3 days of VE/Epi rosette formation, Lif/- indicates Lif supplementation during first 3 days of PrE-induction, -/- indicates no Lif supplementation. **F)** Effect of Lif on total cavity surface area. **G)** Immunofluorescence image of Lif/Lif supplemented structure depicting labels for Pcx, F-actin, nuclei and *Pdgfrα-h2b-gfp.*

**Formation of PrE/Epi rosettes in chemically-defined and gel-free culture conditions**

Following the implantation of the blastocyst *in utero*, the VE deposits a laminin-rich basement membrane that polarizes the Epi cells, which triggers the formation of the pro-amniotic cavity (**Figure 3A**) (Li et al., 2003). Such Epi rosettes can form in the absence of PrE cells when ESCs are encapsulated in Matrigel (that mimics the basement membrane) and cultured in serum-containing medium (that provides signaling molecules)(Bedzhov and Zernicka-Goetz, 2014; Moore et al., 2014). We thus tested whether the PrE/Epi structures could functionally generate PrE/Epi rosettes. Upon transfer into plain B27N2 medium, the suspended PrE/Epi structures grew and formed a cavity morphologically resembling the polarized PrE/Epi tissues (**Figure 3A, 3B**). Similar to post-implantation embryos, the Epi-like cells expressed Oct4, accumulated F-actin and Pcx at the apical side to form a cavity (**Figure 3C, D**), while the PrE-like cells produced a laminin basement membrane and polarized as well (Pcx, **Figure 3D**).

Overtime, the cavities increased in size (**Figure S8B**). The process was both efficient (94%) and reproducible (**Figure S8A, S6C**).

**Lif signalling inhibits formation of the pro-amniotic cavity**

The presence of Lif during first 3 and the 6 days of PrE-induction respectively reduced and fully inhibited the formation of the pro-amniotic cavity as seen by the absence of Pcx within the Epi and non-apically located Pcx in the VE (**Figure 3E-G**). Inhibition of apoptosis using Z-vad-fmk did not impair the hollowing of pro-amniotic cavity (**Figure S8C)**. This two processes occur similarly in Matrigel-embedded, serum-cultured ESCs (Bedzhov and Zernicka-Goetz, 2014; Moore et al., 2014).

Altogether, we concluded that, in chemically-defined conditions, a restricted number of signalling pathways (Wnt, Fgf, RA, cAMP) allow for the co-development of PrE-like and Epi-like cells that form a structure resembling the post-implantation stage.

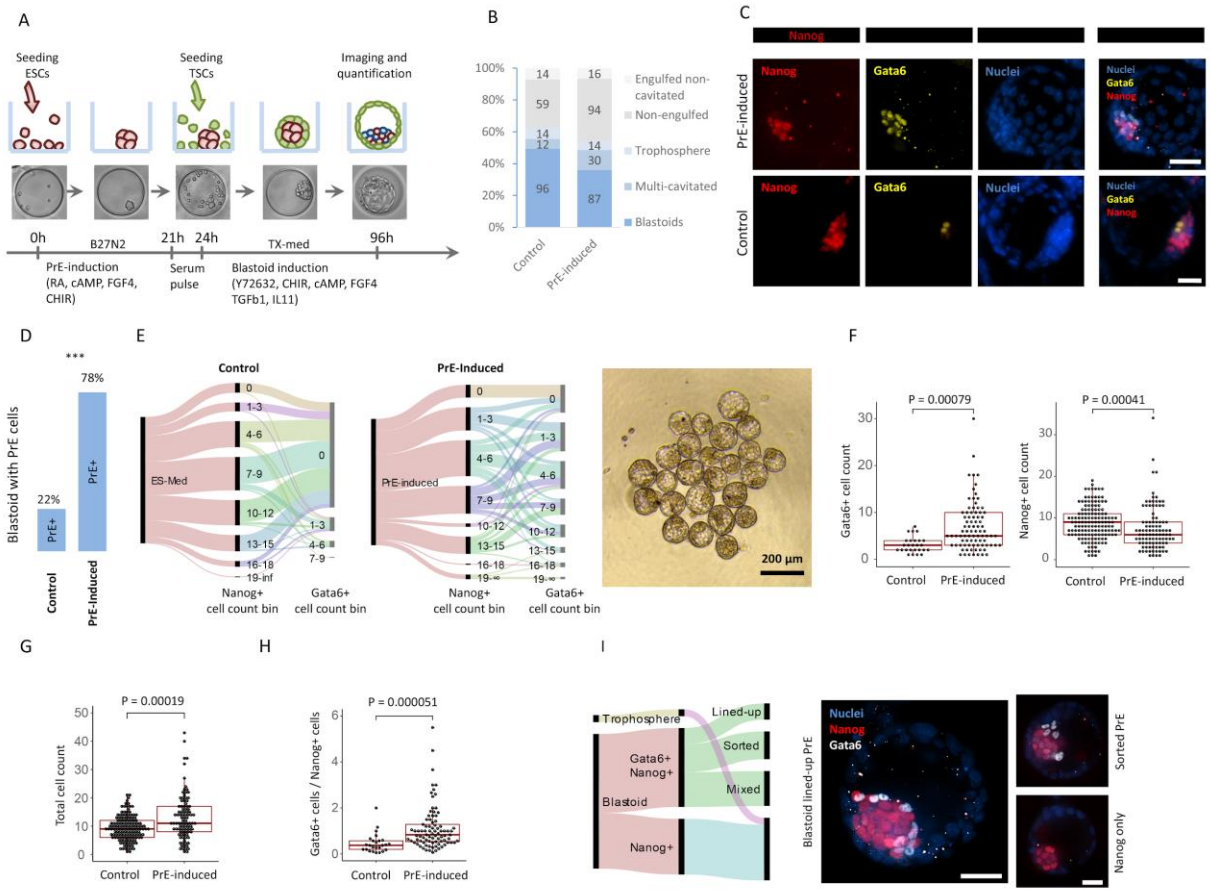


**Figure 4:** The formation of PrE-induced blastoids. A) Schematic of experimental design and stage-specific bright field images of PrE-induced blastoid formation. B) Blastoid formation yields for control and PrE-induced conditions. C) Representative immunofluorescence images of PrE-induced and ES-med blastoids including Nanog+ and Gata6+ cells. Scalebar equals 50 µm. D) Percentage of blastoids including Gata6+/Nanog+ cells, triple asterisks equals $p < 0.001$, Fisher's exact test. Right: brightfield image of selection of PrE-induced blastoids. E) Alluvial diagram displaying cell count of Nanog+ and Gata6+ dichotomy for ES-medium and PrE-induced blastoids. F) Gata6+ and Nanog+ cell counts compared between ES-med and PrE-induced blastoids that contain both Nanog+ and Gata6+ cells. G) Total number of ICM cells (sum of Gata6+ and Nanog+ cells) within blastoids. H) Ratio of Gata6+ / Nanog+ cells per blastoid that contains both Gata6+ and Nanog+ cells. I) Alluvial diagram displaying contributions of resulting phenotypes following PrE-induced blastoid formation. Representative immunofluorescence images of

blastoids with; a lined-up Gata6+ cell epithelium on top of Nanog+ cell cluster (left), sorted PrE but not lined-up (top right) and Nanog+ cells only (bottom right). Images acquired by stacking 3 to 5 spinning disk confocal slides using a 40x objective. Scalebar equals 50 µm.

**Primitive endoderm induction in blastoids.**

Next, we tested the capacity to modulate the induction of PrE-like cells in blastoids by exposing ESCs to the inductive medium during the aggregation phase (0 – 24 hours, **Figure 5A**), and then adding the Trophoblast Stem Cells (TSCs) in blastoid medium (Rivron et al., 2018b). PrE-induction tempered the efficiency of blastoid formation (from 49% to 36%, **Figure 4B**) by reducing the efficiency of TSCs to engulf the EBs (from 39% to 30% of non-engulfed structures, **Figure 4B**). Nevertheless, the induction increased the percentage of blastoids including Gata6+/Nanog+ cells (from 22% to 78%, **Figure 4D, E**), whose number of Gata6+ cell increased (1.6-fold, p-value = 0.00079, **Figure 4E, F).** Notably, the total number of inner cells was higher upon PrE induction (**Figure 4G**). In accordance with a previous study (Saiz et al., 2016), this data confirms that a synergy between PrE and Epi cells regulates the total number of inner cells. The ratio of Gata6+/ Nanog+ cell numbers in PrE-induced blastoids was comparable to the one in blastocyst (0.83 vs. 0.9 in 120 cells-stage blastocyst ((Saiz et al. 2016), **Figure 4H**). When blastocyst progress, the PrE cells sort out from the Epi cells to line the blastocoel cavity. We observed that 21% of the blastoids including PrE-like cells showed a layer of Gata6+ cells lined-up cavity of the blastoid (**Figure 4I)** (Hermitte and Chazaud 2014, Ohnishi et al. 2014). Among the other blastoids, 35% comprised sorted but not lined-up Gata6+ cells, while 44% had a mixed phenotype of Gata6+ and Nanog+ cells reminiscent of earlier blastocysts.

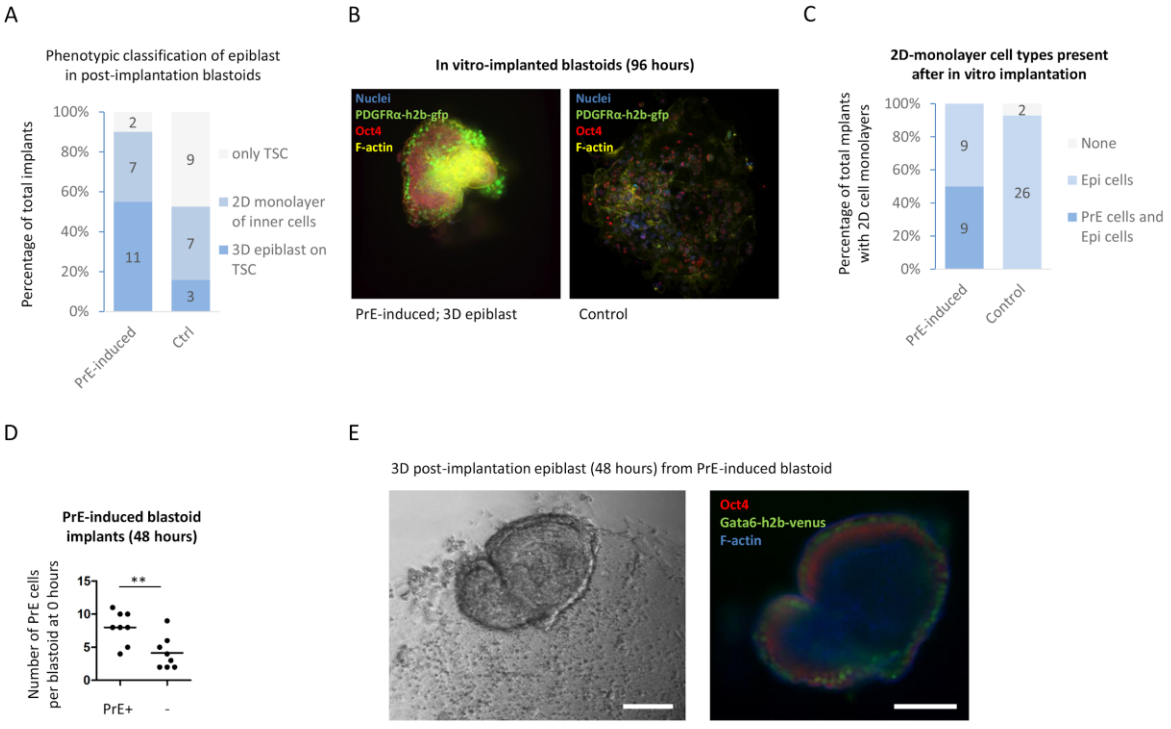


**Figure 5:** Post-implantation competency of PrE-induced blastoids. **A**) Frequency of occurrence of either a TSC monolayer (only TSC), a monolayer of ESC and/or PrE cells on top of TSC monolayer (ESC/PrE on TSC), or a 3-dimensional organization of ESC/PrE, 72 hours after implantation of blastoids *in vitro* on tissue-culture polystyrene dishes. **B**) Representative immunofluorescence images of 3D-structure with Epi (Oct4+) and PrE (Pdgfrα+) cells from in vitro implanted PrE-induced blastoid (left) and a cellular monolayer of in vitro implanted control blastoid (right), 72 hours of implantation). **C)** Presence of 2D-monolayer cell types of the inner cell mass compartment after in vitro implantation of PrE-induced and control blastoids, 48

hours of culture. **D)** The presence of PrE cells at 48 hour PrE-induced blastoid implants compared to the number of PrE cells per blastoid at the moment of implantation, ** denotes $p < 0.01$ student t.test. **E)** Post-implantation epiblast development with Oct4+ and Gata6-h2b-Venus+ cell organization on top of TSC monolayer (48 hours of culture). Scale bars equal 100 µm.

***In vitro* development of post-implantation-like structures from blastoids.**

We then tested whether the PrE/Epi-like tissue within blastoids could support the development of structures reflecting aspects of the post-implantation embryo. We plated PrE-induced blastoids containing PrE cells (>2 $Gata6^{+/h2b\text{-}venus}$ or $Pdgfr\alpha^{+/h2b\text{-}gfp}$ cells) and non-induced blastoids *in vitro* (Bedzhov et al., 2014; Hsu et al., 1974). The viability and expansion of the inner cells was better supported in induced blastoids (90% vs. 58%, **Figure 5a**, monolayer of trophoblasts, 72 hours). In addition, the induction of PrE cells improved the formation of 3D structures (16% vs. 55%, **Figure 5a**) containing Epi and PrE cells (**Figure 5b**). Consistent with our findings in EBs, we concluded that PrE cells are critical for the 3D organization of the post-implantation Epi. When inner cells formed monolayers after implantation, only the induced blastoids permitted an expansion of PrE-like cells (**Figure 5c,** measured by expression of Pdgfrα-h2b-gfp or Gata6-h2b-venus, 48 hours of culture)(**Figure 5c and S10**).
Then, we observed that the potential for the PrE cells to expand after implantation depended on the initial number of PrE cells present in blastoids (**Figure 5d)**. We concluded that PrE-induction promoted the survival of expandable Epi- and PrE-like cells. Finally, upon culture, the PrE-induced blastoids supported the formation of rosettes including Gata6+/ Pdgfrα+ cells surrounding Epi-like cells and including a pro-amniotic-like cavity (2 out of 14 and 1 out of 9 PrE-induced blastoids in two separate experiments, **Figure 5E**). In sharp contrast, the non-induced blastoids lacked that potential.

**Discussion**

High-content screening of large numbers of embryoid bodies in chemically-defined culture conditions allows for robust statistics to delineate the effect of signaling pathways. Here, we observed that the combination of cAMP, RA, Wnt and FGF4 signaling pathways are sufficient to rapidly and efficiently drive the co-formation of PrE-like cells and Epiblast-like cells in gel-free and serum-free cultures. Upon transfer in plain medium, these two cell types are capable of further growing and self-organizing into a structure resembling post-implantation embryonic and extraembryonic tissues.
Consistent with the idea that the blastocyst is a self-regulating system (Saiz et al., 2016), the induction of PrE-like cells in blastoids shows a synergy between PrE and Epi cells regulating the total cell number. This synergy sustains the growth and morphogenetic potential during the post-implantation stage. Accordingly, insufficient differentiation to PrE followed by incomplete lining of the PrE epithelium between the Epi and blastocoel has been described to halt Epi expansion in blastocysts (Artus et al., 2010; Moore et al., 2014). Altogether, these result argue for the importance of the PrE tissue in nurturing the Epi for survival and expansion, and for a synergistic development of the embryonic and extra-embryonic tissues.
Altogether, stem cell-based models of the embryo are amenable to physical and genetic decoupling of cell types and to high-throughput drug and genetic screens while alleviating the burden on the use of animals (Andersson-Rolf et al., 2017; Rivron et al., 2018a). These are foundations of basic and biomedical discoveries.

## Methods and Materials

**Microfabrication**

Elastomeric stamps for imprinting the agarose microwells were fabricated using PDMS Sylgard 184 kit. Microwells were molded using a 2.2% w/v solution of Ultrapure agarose (thermo fisher scientific 11560166) as described

previously (Vrij et al., 2016a). Note for 3D cell cultures: each well of a 96-wellplate contains a total of 430 microwells with a calculated liquid volume of 250 µl split between 225 µl medium and 25 µl hydrogel buffer.

**Stem cell culture**

The following lines were used for experiments: Pdgfrα H2B-GFP/+, V6.5 H2B-RFP V6.5 sub-clone, Gata6 H2B-Venus/+ ;ColA1 TetO-Gata4-mCherry/+ ;R26 M2rtTA/+ ES cells. Gata6 H2B-Venus cell line was a kind gift of C. Schröter' laboratory. The V6.5 cell line has a C57BL/6 X 129/Sv background and was obtained from the laboratory of R. Jaenisch. The Pdgfrα H2B-GFP/+ cell line has an ICR background and was derived from A.-K. Hadjantonakis' laboratory. Standard ES cell expansion was done in 2i/Lif conditions comprising B27N2 (Gibco) medium with leukaemia inhibitory factor (Lif, Merck Millipore ESG1106, 10 ng/ml), PD0325901 (1 µM, AxonMed 1408) and CHIR99021 (3 µM, AxonMed 1386) as developed previously (Nichols et al. 2009), supplemented with 2-mercaptoethanol (Gibco 11528926).

ESCs were seeded and expanded as 25.000 per $cm^2$ on 0.1% w/v gelatin-coated tissue-culture treated polystyrene dishes (Nunc). ESCs were expanded for minimally 2 passages before aggregating into EBs within the agarose microwells.

TSCs were seeded and expanded as 25.000 per $cm^2$ on 3% Matrigel-coated dishes in chemically defined TX-medium as developed previously (Kubaczka et al. 2014) or on TCPS with a Laminin-512 coating (Biolamina LN521-02, 5 µg/ml O/N incubation at 4 degree C) in TX-medium supplemented with Activin-A (Bio-techne 338-AC-010), 50 ng/ml IL11 (Peprotech, 220-11), 200 µM 8Br-cAMP (Biolog, B007-50E), 25 ng/ml BMP7 (RnD systems, 5666-BP-010), 5 nM LPA (Tocris 3854), 2 ng/ml TGFβ1 (Peprotech, 100-21-B), 25 ng/ml FGF4 (RnD systems, 5846-F4-025), 1 µg/ml Heparin (Sigma), 100 µM 2-mercaptoethanol (Gibco 11528926).

**EB, Blastoid and post-implantation culture**

EBs were formed by seeding an average of 7 ESC per microwell in either Serum medium, Serum/Lif medium or B27N2-based media, all supplemented with 50 µM of 2-mercaptoethanol. Serum medium consists of high-glucose DMEM containing sodium pyruvate and Glutamax (Thermofisher, 10569010) and supplemented with 10 mM Non-essential amino acids, 10 mM HEPES and penicillin/streptomycin. Lif was supplemented in a standard working concentration of 10 ng/ml. PrE-induction medium consists of B27N2 medium supplemented with the PrE-induction compounds 3 µM CHIR99021, 50 ng/ml FGF4, 10 nM RA and 1mM 8Br-cAMP and 50 µM 2-mercaptoethanol.

To induce VE/Epi Rosettes from PrE-induced EBs, 14 ESCs per microwell were seeded. Medium was refreshed after 48 hours of culture with B27N2 supplemented with 50 µM of 2-mercaptoethanol. After 72 hours EBs were flushed out and transferred into 6-wellplate wells with 2 ml B27N2 medium and 50 µM of 2-mercaptoethanol.

Blastoids were formed as described previously (Rivron, 2018; Rivron et al., 2018b). For control blastoids, an average of 7 ESC was seeded per microwell in serum/lif medium (10 ng/ml Lif, control blastoids) with 50 µM 2-mercaptoethanol. For PrE-induced blastoids an average of 7 ESC was seeded per microwell in either 1) B27N2 medium with PrE-induction compounds and 10 ng/ml Lif for 21 hours incubation followed by serum/lif for 3 hours, or 2) Serum/Lif medium with PrE-induction compounds. After 24 hours of ESC aggregation and average of 17 TSC were added per microwell in TX-medium with Non-essential amino acids and the blastoid culture components; 20 µM 27632, 5 µM CHIR99023, 1 mM 8Br-cAMP, 25 nG/mL FGF4, 15 nG/mL TGFβ1, 30 nG/mL IL11, 1 µg/ml heparin, 100 µM 2-mercaptoethanol. After 24 hours an additional 1 mM of 8Br-cAMP was added to the blastoid culture medium.

Blastoids cultured for 96 hours (from seeding ESC) were selected on their morphology (cystic, roundness, presence of inner cell mass) and transferred from microwells onto tissue-culture glass or polystyrene plastic in IVC1 medium using mouth pipetting. IVC1 medium consisted of Advanced DMEM/F12 medium (Fisher Scientific, 11540446) with Non-essential amino acids and Sodium pyruvate, 10% ESC-selected fetal bovine serum, 1/100 Glutamax (Fisher

Scientific, 35050061), pen/strep, 1/100 ITS-X (Fisher Scientific, 10524233), 8 nM β-estradiol (Sigma, E8875), Progesterone (Sigma, P8783), 50 µM 2-mercaptoethanol (Gibco 11528926). Structures were fixated after 48 hours of culture.

**Immunofluorescence**

Blastoids and blastocysts were fixated in 4% paraformaldehyde solution in 1X PBS for 15 minutes at room temperature. VE/Epi rosettes and in vitro implantation cultures were fixated in 2% paraformaldehyde solution with 0.1% glutaraldehyde in 1X PBS for 15 minutes at room temperature. After fixation, samples were washed 3x in washing buffer (0.1% Triton-X with 2% BSA in 1xPBS), permeabilized in 1% Triton-X solution in 1xPBS and blocked in blocking buffer (2% BSA, 5% serum of host 2nd antibody species, 0.5% glycine, 0.1% Triton-X, 0.2% Tween-20) for 30 minutes. Samples were incubated in antibody solution (¼ of blocking buffer with ½ of 1xPBS and ¼ of 0.1% Triton-X in 1xPBS) with primary antibodies for 12 hours at 4 degree C, washed 3x 10 minutes with washing buffer followed by incubation with secondary antibodies in antibody solution for 4 hours at 4 degree C. Dapi (0.2 ug/ml) and phalloidin (Thermo Scientific, 1/100 dilution).

**Antibody list**

- Mouse Podocalyxin, RnD systems AF1556, 1/300 dilution
- Human/mouse Oct-3/4, RnD systems AF1759, 1/150 dilution
- Human Sox17, RnD systems AF1924, 1/150 dilution
- Anti-Laminin antibody produced in rabbit, Sigma Aldrich L9393, 1/100 dilution
- Anti-Nanog antibody (Abcam ab80892), 1/150 dilution
- Anti-Gata6 (mouse/human) poly Goat (AF1700) 200uG/mL, 1/200 dilution
- Goat anti-mouse IgM heavy chain secondary antibody, AF568 Invitrogen 10614383, 1/500 dilution
- Goat anti-Rabbit IgG (H+L) Secondary Antibody, Alexa Fluor® 488 conjugate, 1/500 dilution
- Alexa Fluor® 647 Goat Anti-Mouse IgG (H+L) Antibody, highly cross-adsorbed, 1/500 dilution
- Alexa Fluor® 568 Goat Anti-Mouse IgG (H+L) Antibody, highly cross-adsorbed, 1/500 dilution
- Donkey anti-Goat IgG (H+L) Secondary Antibody, Alexa Fluor® 647 conjugate, 1/500 dilution
- Goat anti-Rabbit IgG (H+L) Secondary Antibody, Alexa Fluor 647, 1/500 dilution

**Soluble factors**

- Mouse recombinant FGF-4 protein, RnD systems 5846-F4
- Y-27632 dihydrochloride, RnD systems 1254/10
- PD0325901 (AxonMed 1408)
- CHIR99021 (AxonMed 1386)
- Recombinant human TGF-B1, Peprotech 100-21
- Recombinant murine Noggin, Peprotech 250-38
- Recombinant murine BMP-4, Peprotech 315-27
- Recombinant mouse BMP-7, R&D systems 5666-BP-010
- Recombinant mouse Nodal, R&D systems 1315-ND-025
- Recombinant Murine IL-11, Peprotech 220-11
- Recombinant Murine IL-6, Peprotech 216-16
- ML347, Selleckchem S7148
- Sodium orthovanadate, Sigma Aldrich S6508
- LDN 193189
- IWP2
- XAV 939

- SC144, RnD systems 4963 /10
- PD98059, Sigma P215
- Sodium (Ortho)Vanadate, Sigma S6508
- Retinoic acid, Sigma R2625
- SB431542, Tocris 1614
- DL-Epinephrine HCl (DL-Adrenaline), Sigma E4642
- A83-01, Tocris 2939

**Data analysis**

Alluvial figures were created using RAW - an open source project by DensityDesign Lab and Calibro. Clustering analysis and heatmaps were made using R (Team and Others, 2013). Bar plots were made using Microsoft Excel. SPRING Louvain clustering was performed using Kleintools (Weinreb et al., 2016).

## References

Andersson-Rolf, A., Mustata, R.C., Merenda, A., Kim, J., Perera, S., Grego, T., Andrews, K., Tremble, K., Silva, J.C.R., Fink, J., et al. (2017). One-step generation of conditional and reversible gene knockouts. Nat. Methods *14*, 287–289.

Artus, J., Panthier, J.-J., and Hadjantonakis, A.-K. (2010). A role for PDGF signaling in expansion of the extra-embryonic endoderm lineage of the mouse blastocyst. Development *137*, 3361–3372.

Bedzhov, I., and Zernicka-Goetz, M. (2014). Self-organizing properties of mouse pluripotent cells initiate morphogenesis upon implantation. Cell *156*, 1032–1044.

Bedzhov, I., Leung, C.Y., Bialecka, M., and Zernicka-Goetz, M. (2014). In vitro culture of mouse blastocysts beyond the implantation stages. Nat. Protoc. *9*, 2732–2739.

Brickman, J.M., and Serup, P. (2017). Properties of embryoid bodies. Wiley Interdiscip. Rev. Dev. Biol. *6*.

Calebiro, D., and Jobin, M.-L. (2018). Hot spots for GPCR signaling: lessons from single-molecule microscopy. Curr. Opin. Cell Biol. *57*, 57–63.

Chazaud, C., Yamanaka, Y., Pawson, T., and Rossant, J. (2006). Early lineage segregation between epiblast and primitive endoderm in mouse blastocysts through the Grb2-MAPK pathway. Dev. Cell *10*, 615–624.

Cho, L.T.Y., Wamaitha, S.E., Tsai, I.J., Artus, J., Sherwood, R.I., Pedersen, R.A., Hadjantonakis, A.-K., and Niakan, K.K. (2012). Conversion from mouse embryonic to extra-embryonic endoderm stem cells reveals distinct differentiation capacities of pluripotent stem cell states. Development *139*, 2866–2877.

Doetschman, T.C., Eistetter, H., Katz, M., Schmidt, W., and Kemler, R. (1985). The in vitro development of blastocyst-derived embryonic stem cell lines: formation of visceral yolk sac, blood islands and myocardium. J. Embryol. Exp. Morphol. *87*, 27–45.

Edgar, R., Mazor, Y., Rinon, A., Blumenthal, J., Golan, Y., Buzhor, E., Livnat, I., Ben-Ari, S., Lieder, I., Shitrit, A., et al. (2013). LifeMap Discovery™: the embryonic development, stem cells, and regenerative medicine research portal. PLoS One *8*, e66629.

Gardner, R.L. (2000). Flow of cells from polar to mural trophectoderm is polarized in the mouse blastocyst. Hum. Reprod. *15*, 694–701.

Hamazaki, T., Oka, M., Yamanaka, S., and Terada, N. (2004). Aggregation of embryonic stem cells induces Nanog

repression and primitive endoderm differentiation. J. Cell Sci. *117*, 5681–5686.

Hsu, Y.C., Baskar, J., Stevens, L.C., and Rash, J.E. (1974). Development in vitro of mouse embryos from the two-cell egg stage to the early somite stage. J. Embryol. Exp. Morphol. *31*, 235–245.

Hutchens, S.A., León, R.V., O'neill, H.M., and Evans, B.R. (2007). Statistical analysis of optimal culture conditions for Gluconacetobacter hansenii cellulose production. Lett. Appl. Microbiol. *44*, 175–180.

Krawetz, R., and Kelly, G.M. (2008). Wnt6 induces the specification and epithelialization of F9 embryonal carcinoma cells to primitive endoderm. Cell. Signal. *20*, 506–517.

Li, S., Edgar, D., Fässler, R., Wadsworth, W., and Yurchenco, P.D. (2003). The Role of Laminin in Embryonic Cell Polarization and Tissue Organization. Dev. Cell *4*, 613–624.

Mesnard, D., Guzman-Ayala, M., and Constam, D.B. (2006). Nodal specifies embryonic visceral endoderm and sustains pluripotent cells in the epiblast before overt axial patterning. Development *133*, 2497–2505.

Moore, R., Tao, W., Smith, E.R., and Xu, X.-X. (2014). The primitive endoderm segregates from the epiblast in β1 integrin-deficient early mouse embryos. Mol. Cell. Biol. *34*, 560–572.

Morgani, S.M., and Brickman, J.M. (2015). LIF supports primitive endoderm expansion during pre-implantation development. Development *142*, 3488–3499.

Niakan, K.K., Schrode, N., Cho, L.T.Y., and Hadjantonakis, A.-K. (2013). Derivation of extraembryonic endoderm stem (XEN) cells from mouse embryos and embryonic stem cells. Nat. Protoc. *8*, 1028–1041.

Onishi, K., and Zandstra, P.W. (2015). LIF signaling in stem cells and development. Development *142*, 2230–2236.

Plusa, B., Piliszek, A., Frankenberg, S., Artus, J., and Hadjantonakis, A.-K. (2008). Distinct sequential cell behaviours direct primitive endoderm formation in the mouse blastocyst. Development *135*, 3081–3091.

Price, F.D., Yin, H., Jones, A., van Ijcken, W., Grosveld, F., and Rudnicki, M.A. (2013). Canonical Wnt signaling induces a primitive endoderm metastable state in mouse embryonic stem cells. Stem Cells *31*, 752–764.

Rivron, N. (2018). Formation of blastoids from mouse embryonic and trophoblast stem cells.

Rivron, N., Pera, M., Rossant, J., Martinez Arias, A., Zernicka-Goetz, M., Fu, J., van den Brink, S., Bredenoord, A., Dondorp, W., de Wert, G., et al. (2018a). Debate ethics of embryo models from stem cells. Nature *564*, 183–185.

Rivron, N.C., Frias-Aldeguer, J., Vrij, E.J., Boisset, J.-C., Korving, J., Vivié, J., Truckenmüller, R.K., van Oudenaarden, A., van Blitterswijk, C.A., and Geijsen, N. (2018b). Blastocyst-like structures generated solely from stem cells. Nature *557*, 106–111.

Saiz, N., Williams, K.M., Seshan, V.E., and Hadjantonakis, A.-K. (2016). Asynchronous fate decisions by single cells collectively ensure consistent lineage composition in the mouse blastocyst. Nat. Commun. *7*, 13463.

Schrode, N., Saiz, N., Di Talia, S., and Hadjantonakis, A.-K. (2014). GATA6 levels modulate primitive endoderm cell fate choice and timing in the mouse blastocyst. Dev. Cell *29*, 454–467.

Schröter, C., Rué, P., Mackenzie, J.P., and Martinez Arias, A. (2015). FGF/MAPK signaling sets the switching threshold of a bistable circuit controlling cell fate decisions in embryonic stem cells. Development *142*, 4205–4216.

Team, R.C., and Others (2013). R: A language and environment for statistical computing.

Vrij, E., Rouwkema, J., LaPointe, V., van Blitterswijk, C., Truckenmüller, R., and Rivron, N. (2016a). Directed Assembly and Development of Material-Free Tissues with Complex Architectures. Adv. Mater. *28*, 4032–4039.

Vrij, E.J., Espinoza, S., Heilig, M., Kolew, A., Schneider, M., van Blitterswijk, C.A., Truckenmüller, R.K., and Rivron, N.C. (2016b). 3D high throughput screening and profiling of embryoid bodies in thermoformed microwell plates. Lab Chip *16*, 734–742.

Weinreb, C., Wolock, S., and Klein, A. (2016). SPRING: a kinetic interface for visualizing high dimensional single-cell expression data.

Yamanaka, Y., Lanner, F., and Rossant, J. (2010). FGF signal-dependent segregation of primitive endoderm and epiblast in the mouse blastocyst. Development *137*, 715–724.

## Supplementary information

S1A

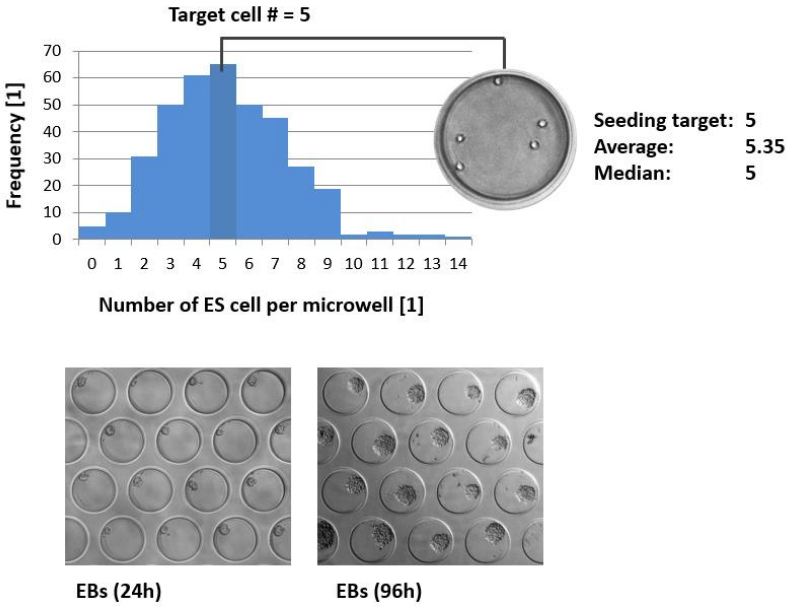

S1B

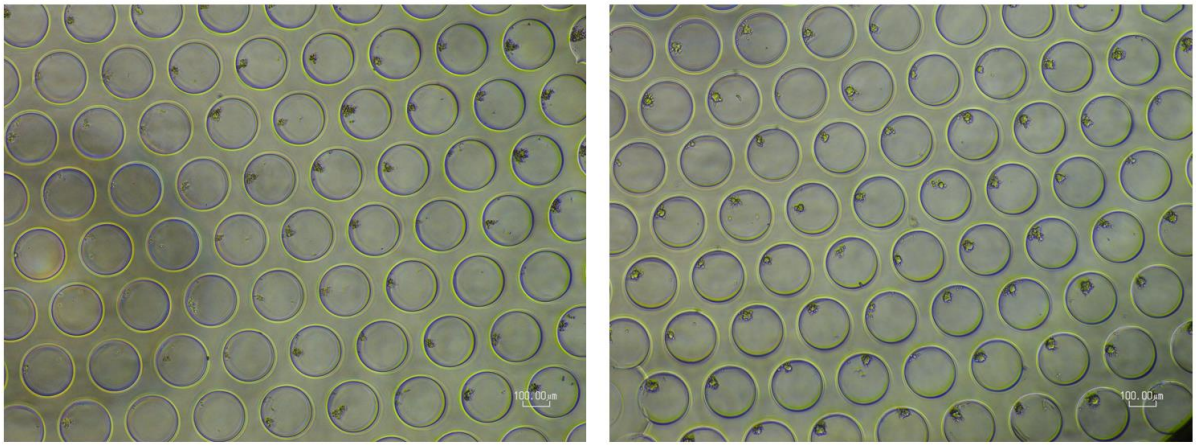

B27N2 B27N2 with Lif

EBs formed from an average of 5 ESC per microwell (72 hours).

S2

A – Pipeline for image-based analysis of PrE-differentiation

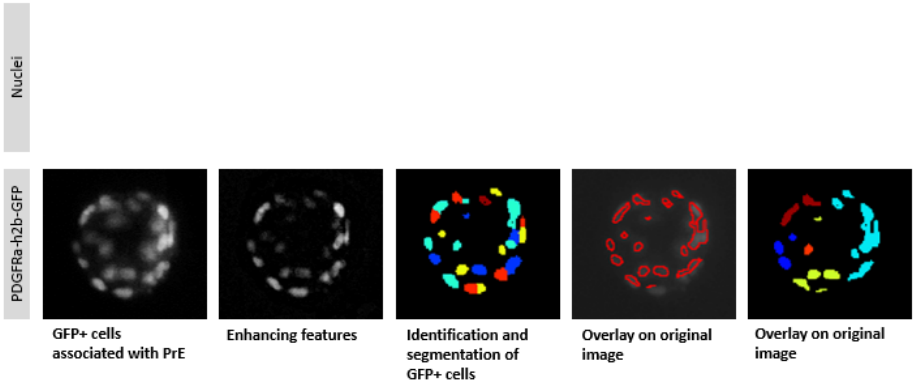


Pipeline for identification, segmentation and quantification of GFP+ cells within EBs.

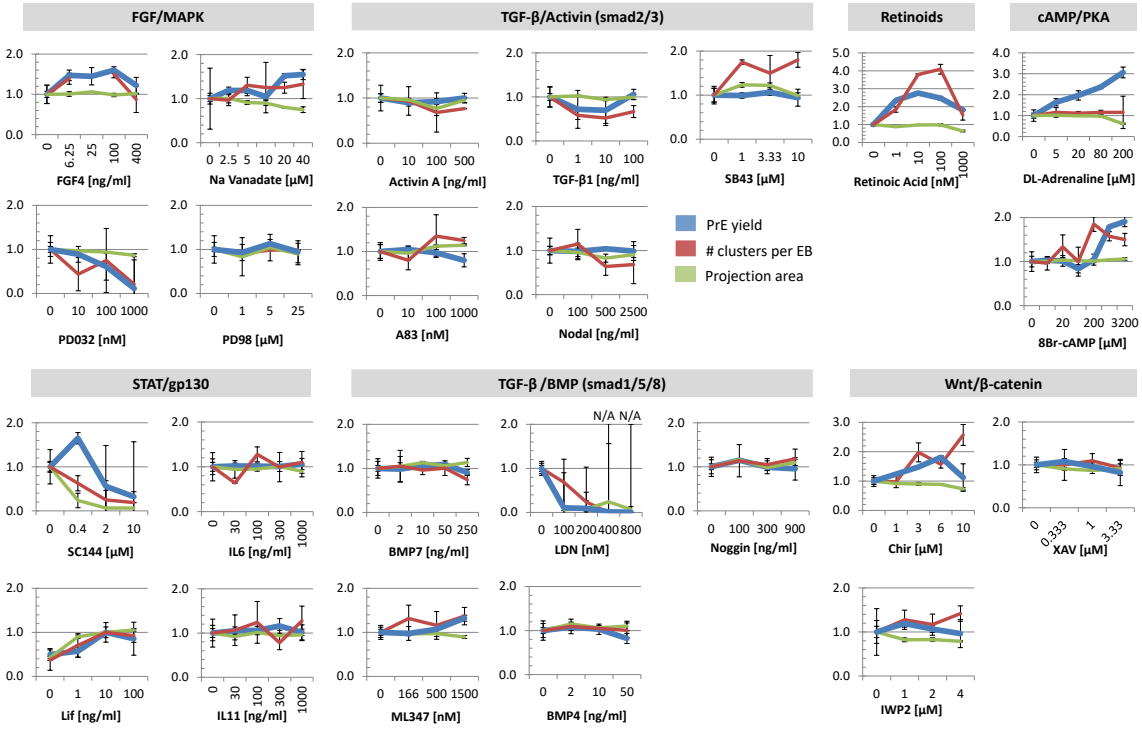


**Modulating signal transduction pathways involved in primitive endoderm differentiation.** Values are depicted for the percentage of GFP+ EBs as the PrE-yield (blue), number of PrE cells per EB (red) in median focus plane (10x objective) and projection area as a proxy for EB-size (green). All values were normalized to H20/DMSO controls. Average and standard deviation values were obtained from n = 4 wells with every well containing approximately 400 EBs.

A – Definitive Screening Design of 9 factors

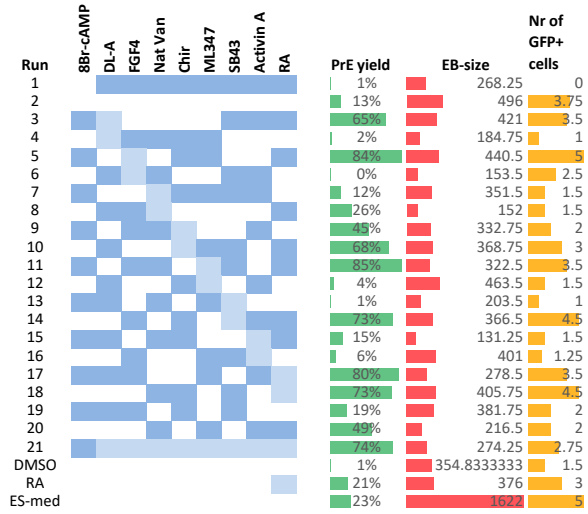


B – Combinatorial screening in B27N2/Lif

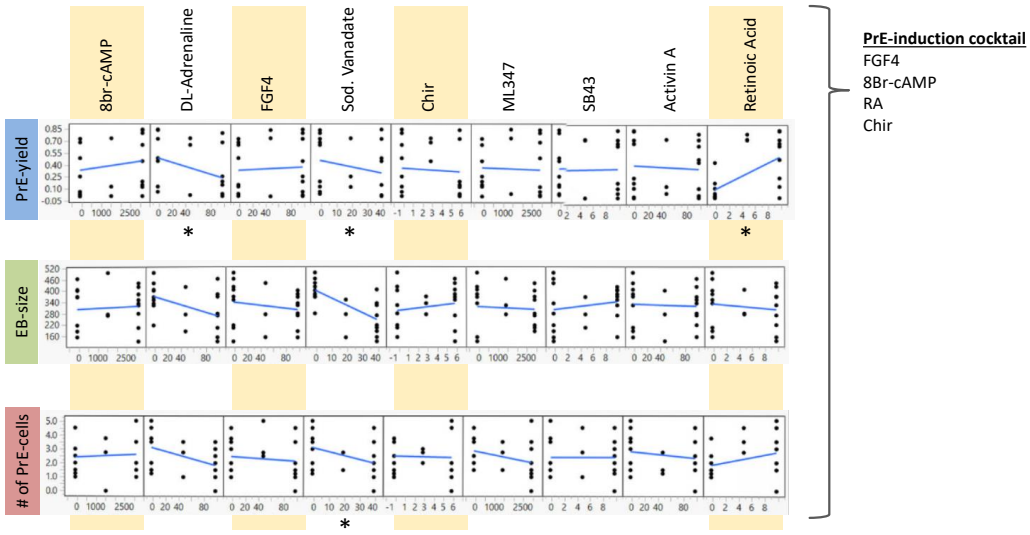


Combinatorial screening for serum-free differentiation into primitive endoderm.

a) Experimental layout of Definitive Screening Design and the results of factor combinations on the yield of PrE-differentiation in EBs (PrE-yield), EB projection area (EB-size) and number of GFP+ cells per EB (Nr of GFP+ cells).

b) Main effect plots for the 9 factors in the combinatorial definitive screening design (DSD) assay shows a positive correlation with PrE-yield for 8Br-cAMP, FGF4 and RA, a positive correlation with EB-size for Chir, SB43 and 8Br-cAMP, and a positive correlation with the number of PrE+ cells for RA. All conditions were supplemented with Lif and β-mercaptoethanol. Asterisks indicate statistical significance. Yellow-marked compounds; FGF4, 8Br-cAMP, RA and Chir were selected for final induction cocktail.

S5

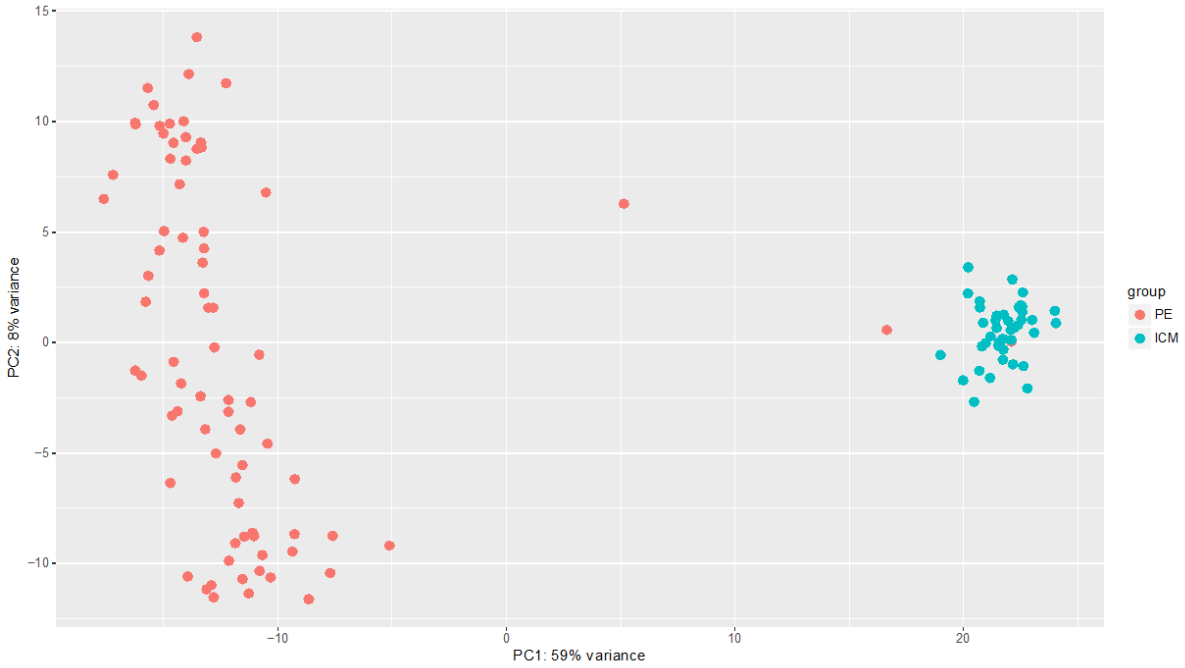


Principal component analysis on snSeq data of PrE-induced EBs.

S6

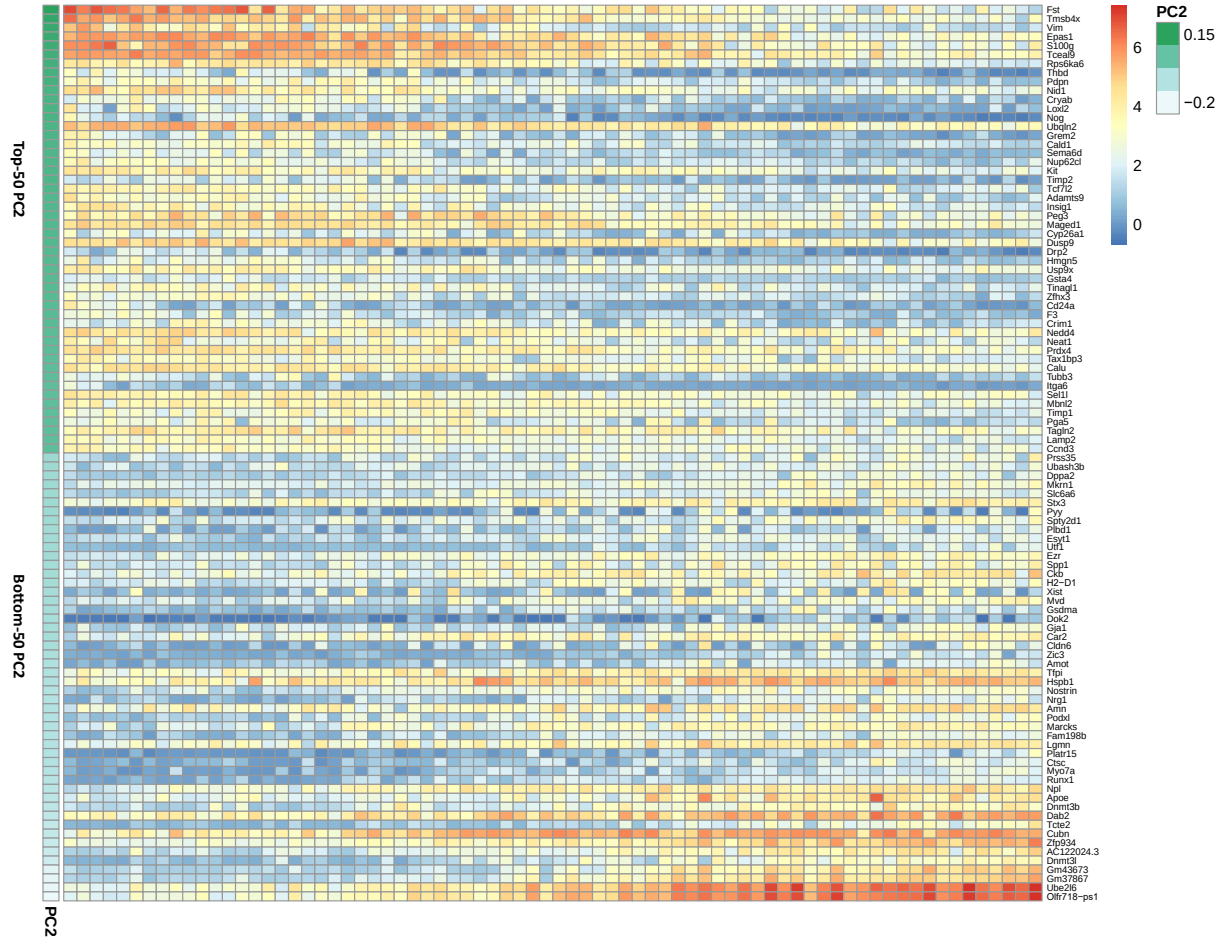


PrE cells (positive for PDGFRα-antibody labelling) order by PC2 value; Top 50 genes and bottom 50 genes

S7

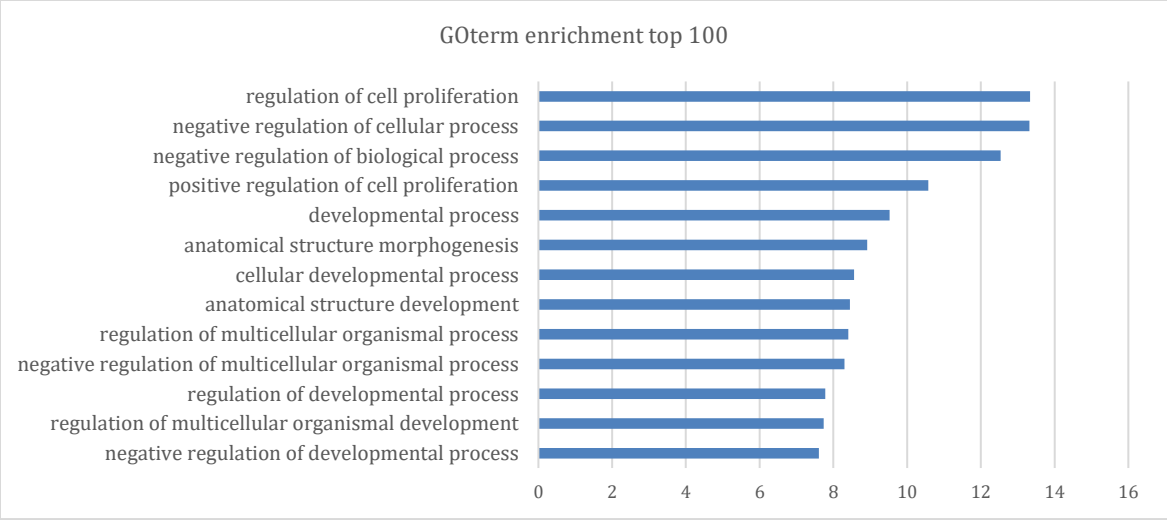


GOterm enrichment ranking for upregulated genes in the putative VE subpopulation.

S8

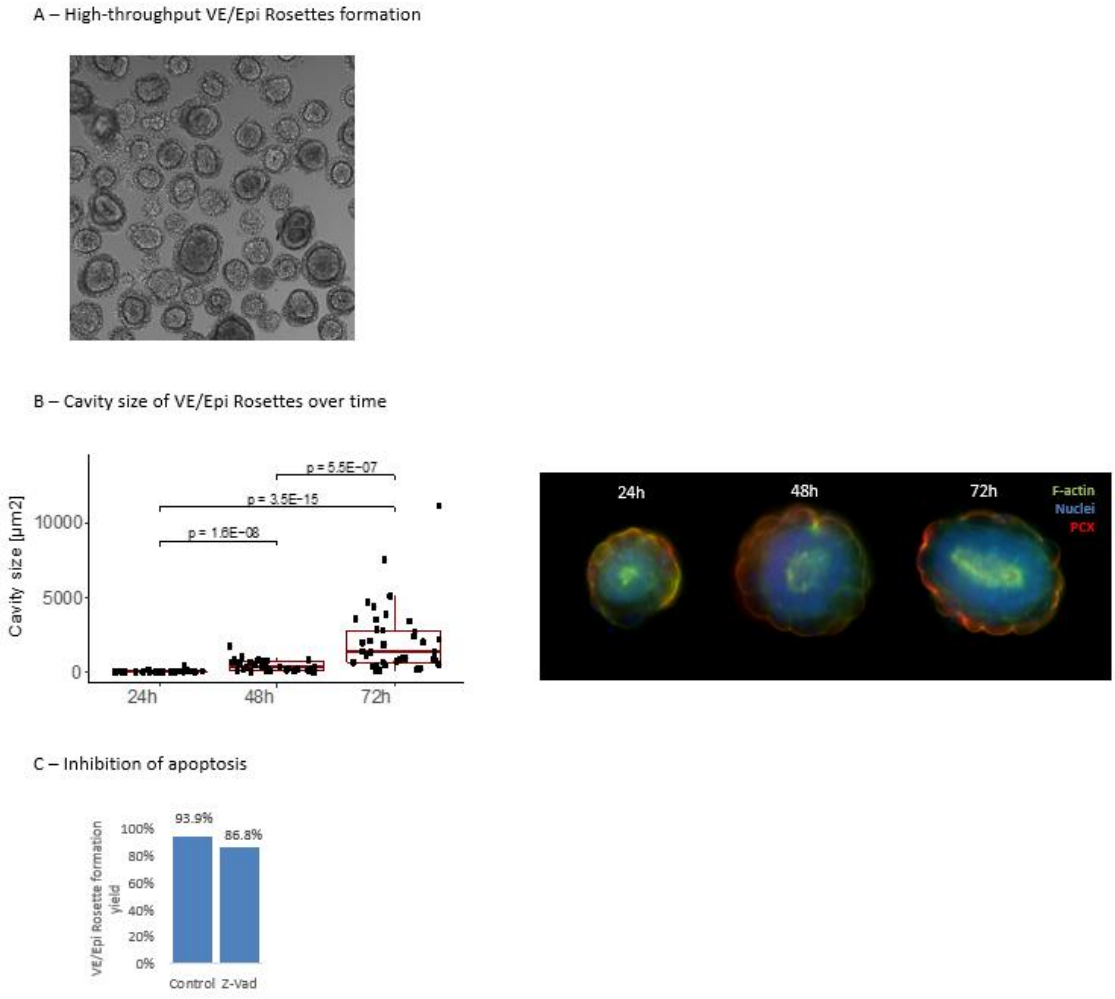

A) High-throughput formation of VE/Epi rosettes using PrE-induction factors in B27N2 medium (average of 24 ESCs per microwell, brightness-adjusted bright-field image). B) Size of cavities in VE/Epi Rosettes over time. C) Formation efficiency of VE/Epi Rosettes containing pro-amniotic-like cavities with and without addition of apoptotic inhibitor Z-vad-fmk (Z-Vad). P-values were calculated according to the Mann – Whitney U test.

S9

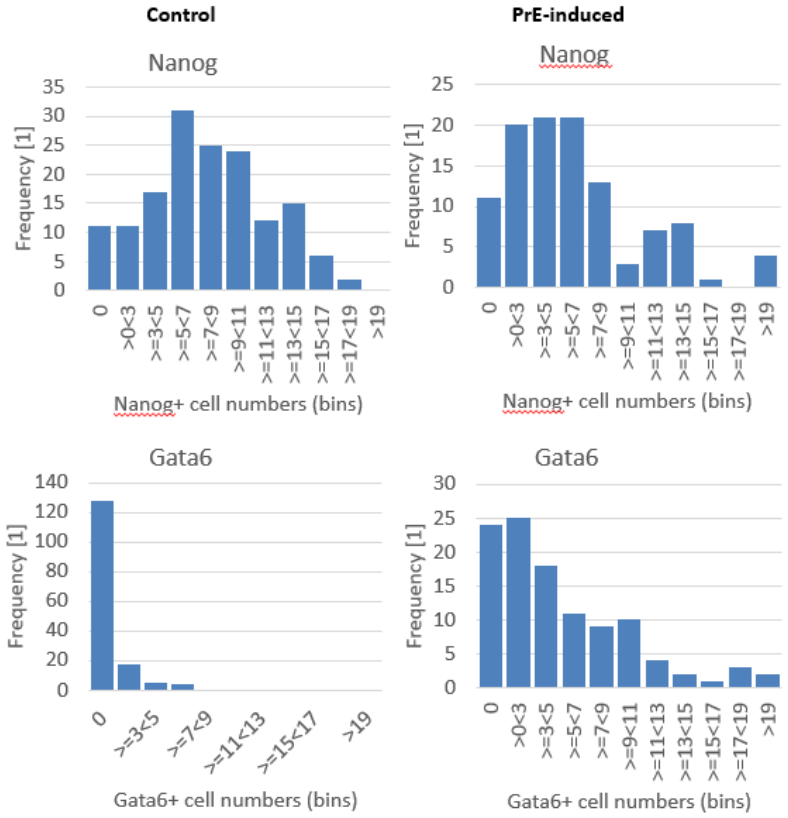


Histograms showing occurrences of different Nanog+ and Gata6+ cell numbers within control and PrE-induced blastoids.

S10

**Implant of non-PrE-induced blastoid (48h)**

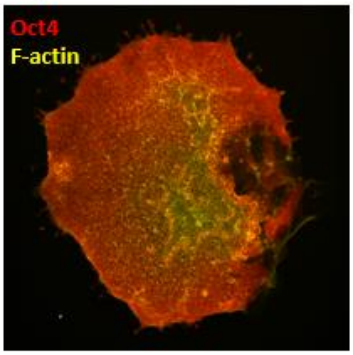


Control; ESC on TSC

2-dimensional (monolayer) outgrowth of Oct4+ ESCs from control blastoid implant (48h).